Holographic light scattering in centrosymmetric sodium nitroprusside upon generation of light-induced metastable states

M. Imlau,* M. Fally,† T. Weisemoeller, and D. Schaniel
Fachbereich Physik, Universität Osnabrück, Barbarastrasse 7, D-49069 Osnabrück, Germany

P. Herth and Th. Woike
Institut für Mineralogie und Geochemie, Universität zu Köln, Zülpicherstrasse 49b, D-50674 Köln, Germany
(Received 16 December 2005; published 22 May 2006)

The phenomenon of holographic light scattering in centrosymmetric crystals of sodiumnitroprusside is investigated by analyzing (1) the effect of light polarization and wavelength of pump- and readout beams, (2) the angular intensity distribution, and (3) the kinetics of scattered light. It is shown that the scattering phenomenon and the corresponding properties can be entirely explained by diffraction processes of the pump beam from parasitically recorded slanted phase gratings without assuming any beam-coupling processes. The kinetics originates from the nonlinear photorefractive recording mechanism. Further we present an approach for three-wave interaction including diffraction processes at higher harmonics, that explains the temporal build-up of wide-angle scattering in media with a nonlinear photorefractive response.

DOI: 10.1103/PhysRevB.73.205113 PACS number(s): 42.40.−i, 42.65.Pc, 42.70.Ln, 78.35.+c

I. INTRODUCTION

The phenomenon of nonlinear light scattering occurs when exposing photorefractive crystals to coherent laser light. The formation of intensely scattered light into a wide apex angle as well as of characteristic scattering patterns such as rings and lines is observed around the directly transmitted laser beam. Since the discovery of photorefraction in 1966 (Ref. 1) the appearance of nonlinear light scattering is reported in various photorefractive materials, such as electrooptic media,[2] films,[3] photopolymers,[4] composite media from polymers and liquid crystals,[5] ceramics,[6] and centrosymmetric crystals.[7] The phenomenon originates from diffraction of the incoming laser beam at parasitically recorded holographic phase gratings. Thus it is called "holographic light scattering" or, provided that there is a feedback between recording and read-out process, "photoinduced light scattering."[8] Although nonlinear light scattering is claimed to be a serious drawback for many applications it is increasingly employed as a comprehensive tool for the analysis of photorefractive materials in the field of material science.[9]

Still the phenomenon keeps a couple of physical facts in private that hinders overall understanding, such as the origin and properties of initially scattered light. In this article we focus on the open questions connected to holographic light scattering in centrosymmetric crystals. In particular we investigate the processes that are responsible for the formation of a pronounced scattering intensity distribution into all directions of space in centrosymmetric photorefractive crystals of sodium nitroprusside (SNP). The specific importance of SNP is related to its representative character for a variety of compounds described by the composition $X\cdot[ML_5\mathrm{NO}]\cdot y\mathrm{H_2O}$, with the central atom $M=\mathrm{Fe,Ru,Os,Ni,Mo}$, ligands L, e.g., $L=\mathrm{F^-,Cl^-,Br^-,I^-,OH^-,CN^-,NH_3,C_2O_4^-}$, various counter ions such as $X=\mathrm{Na^+,K^+,Rb^+,Cs^+,Mg^{2+},Ca^{2+},Sr^{2+},Ba^{2+},Cl^-,Br^-,NH_4^+,CN_3H_6^+}$, and different amounts of crystal water y.[10–13] Due to the well-known activity of the NO molecule, this material group offers important biological functions like neurotransmission, penile erection, enzyme, immune and blood pressure regulation, and even inhibition of tumor growth.[14–16] Photorefraction is expected in most of these compounds which uncovers an unusual but powerful tuning ability of the photorefractive properties by variation of the chemical composition.[17] For this purpose, the analysis of holographic light scattering at the example of SNP can be brought forward to novel photorefractive $X\cdot[ML_5\mathrm{NO}]\cdot y\mathrm{H_2O}$ compounds yielding insight into their photorefractive properties.

In order to highlight the specific problem we briefly recall at first the standard model for holographic light scattering:[18] it emerges from initial scattering of an incident coherent laser beam at inhomogeneities within the photorefractive material or on its surface. The complex interference pattern formed by the incident and initially scattered waves is transferred into small refractive-index changes via the photorefractive effect. Subsequently, diffraction of the pump beam occurs and scattered light is observed around the directly transmitted laser beam. If the initially scattered and the diffracted waves are in phase, the scattered light continuously increases by two-wave mixing.[19] Thus this condition is connected to photorefractive materials with a nonlocal photorefractive response, i.e., media with a phase shift between refractive-index and light intensity modulation. As a result scattered light is formed in a preferred direction commonly designated as photoinduced light scattering.[8] Contrary, the photorefractive response in centrosymmetric crystals must be local due to symmetry considerations,[20] which is consistent with the observation of a broad scattering pattern formed along all directions. However, the initially scattered waves cannot be amplified by beam coupling and thus light amplification in centrosymmetric materials must have a different origin that is still not identified.

Here, we investigate the spatial intensity distribution and the kinetics of the scattering pattern in centrosymmetric SNP to gain a first insight into the recording mechanism. Equivalent investigations performed in acentric photorefractive

crystals yielded valuable information especially on photoinduced light scattering in electro-optic materials.[21–23] It is already established that light illumination causes a change of the refractive index in SNP and related substances. The physical origin is connected to the generation of two long-lived metastable electronic states,[20,24] commonly denoted as SI and SII, undergoing light-induced charge redistributions at the local $[Fe(CN)_5NO]^{2-}$-anion.[25] Note, that the linear electrooptic effect is forbidden because of symmetry in centrosymmetric crystals and cannot be responsible for photorefraction as in electrooptic crystals such as $LiNbO_3$.[26] The coefficients of the quadratic electrooptic effect are negligible in SNP. Beside a wide-angle polarization-isotropic scattering distribution the phenomenon of holographic light scattering in SNP demonstrably occurs with a number of astonishing facets such as the build-up of anisotropic scattering cones.[27]

The pertinence of our investigations is twofold. First the aspect of material characterization using holographic light scattering can be extended to a variety of photorefractive media, such as glasses, polymers, films, and further centrosymmetric crystals. Secondly, the formation of holographic light scattering is not restricted to a single direction in space. It should be noted, that centrosymmetric crystals are eligible candidates for photonic applications, such as, e.g., holographic data storage. A deeper knowledge about unwanted nonlinear phenomena will open up new possibilities for the effective usage of these promising materials.

Our experiments reveal three remarkable features. (a) The possibility to control the appearance of the scattering pattern via the light polarization of the read-out beam. (b) The spatial intensity distribution of the scattering pattern represents a broad concentric ring around the transmitted laser beam. (c) The overall scattered intensity increases and subsequently decreases as a function of exposure, i.e., it shows a transient behavior.

Here, we show that the spatial intensity distribution results from the angular dependence of the diffraction efficiency for slanted holographic phase gratings. The kinetic behavior is found to originate from the nonlinear photorefractive recording mechanism. An approach for three-wave interaction including diffraction processes at higher harmonics is presented, that explains the build-up of wide-angle scattering in media with nonlinear photorefractive response.

II. EXPERIMENTAL SETUP

Crystals of SNP, $Na_2[Fe(CN)_5NO]\cdot 2H_2O$, space group *Pnnm*,[28] were grown from aqueous solution and cut perpendicular to the crystallographic axes. Specimens with dimensions of 10×10 mm^2 and thicknesses between 0.1 and 0.5 mm are polished with Cr_2O_3 to optical quality and are mounted onto a sample holder diving into a nitrogen-filled Dewar. Optical access to the sample is realized via four flat plane-parallel windows of optical quality. The sample holder is mounted onto a motorized rotary stage for crystal rotation. The temperature of the sample is kept constant at 100 K during all experiments.

The light of an argon-ion laser, a Nd:YAG laser, a HeNe laser, or a GaAlAs laser impinges onto the crystal plate orthogonally to its surface (Fig. 1). Intensity and polarization of the laser light are adjusted by a combination of $\lambda/2$ retarders and Glan-Thompson polarizers. Laser action and stability are controlled by an electromechanical shutter and a Si-PIN-diode D3, respectively. Intensity and polarization of the directly transmitted laser beam are detected as a function of time with a Si-PIN diode D2. The spatial scattering intensity distribution is investigated in one dimension within an apex angle of ±25° using Si-PIN diode D1 mounted onto a motorized linear stage as illustrated in Fig. 2.

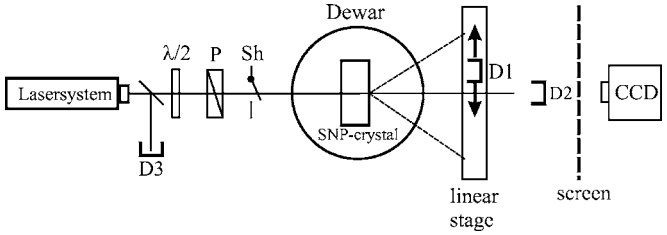

FIG. 1. Experimental setup for the study of scattering in SNP. Various laser systems were used: argon-ion laser (λ=457.9, 476.5, 488, 501.7, 514.5 nm), Nd:YAG-laser (λ=532, 1064 nm), HeNe-laser (λ=632.8 nm), and GaAlAs-Laser (λ=785 nm). D1-D3: Si-PIN diodes, λ/2: wave retarder plate P: Glan-Thompson polarizer, Sh: shutter.

As an example a scan direction parallel to the crystallographic *b* axis is shown (dotted line) for a scattering pattern obtained with a *c* cut of SNP of thickness $d=210$ μm ($\lambda=532$ nm, $\vec{E}_p \| a$). The two-dimensional intensity distribution is recorded with a CCD array. The advantage of the Si-PIN diode over the array is its extremely large dynamic range.

III. EXPERIMENTAL RESULTS

In a first step the role of light polarization and wavelength on the formation of holographic light scattering in SNP is investigated. The observed scattering patterns for the principal configurations of light polarizations of pump $\vec{E}_p$ and read-out beams $\vec{E}_r$ with respect to the orthorhombic crystal system are shown in Fig. 3.

Note that the crystal was exposed to light of wavelength $\lambda_p=532$ nm up to $Q=100$ W s/cm^2 prior to taking a photo of the intensity distributions with an attenuated pump beam. Rows 1–3 correspond to light polarizations $\vec{E}_p$ of the pump

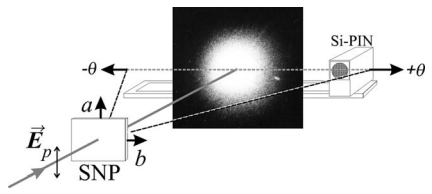

FIG. 2. Schematic illustration of the orientation of the scattering distribution (photograph) with respect to the crystallographic axes for a *c* cut. Light polarization is chosen $\vec{E}_p \| a$, the scan is performed along the *b*-axis direction. The external apex angle is limited to a range of ±25° with a spatial resolution of 0.2°. The Si-Pin diode is equipped with an iris diaphragm of diameter 1.0 mm.

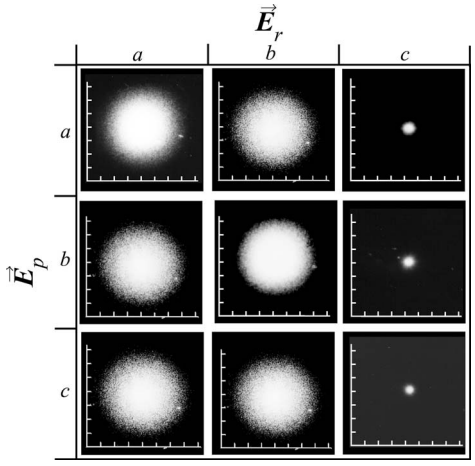

FIG. 3. Far-field photographs of the scattering distributions taken on a screen behind the crystal after an exposure of 100 W s/cm^2 at λ_p=532 nm and light polarizations of the pump and read-out beams parallel to the *a*, *b*, and *c* axis, respectively.

beam parallel to the *a*, *b*, and *c* axis, respectively. Columns 1–3 denote the orientation of the electric field vector $\vec{E}_r$ for read-out parallel to the *a*, *b*, and *c* axis, respectively. Obviously, the appearance of the scattering pattern after recording depends on the light polarization of the read-out beam: The scattering appears for any light polarization of the pump beam, presumed a light polarization of the read-out beam $\vec{E}_r \| a$ or *b* axis. Increasing the pre-exposure until saturation at about Q=3000 W s/cm^2 does not reveal any difference. The holographic nature of the scattering was proven by a slight rotation of the crystals with respect to the read-out beam (about 15°), so that the Bragg condition was violated and hence the characteristic diffraction ring appeared.[7]

We emphasize that this result comprises a remarkable property: the appearance of holographic scattering in SNP can be controlled by the light polarizations of the read-out beams. Scattering patterns which were recorded with a light polarization parallel to the *a* or *b* axis completely vanish when read out with $\vec{E}_r \| c$ axis (row 1 / column 3; row 2 / column 3). Likewise scattering is visible even after pre-exposure with $\vec{E}_p \| c$ axis (row 3 / column 1; row 3 / column 2) if $\vec{E}_r \| a$ or *b* axis.

In addition the appearance of light-induced scattering was investigated for different wavelengths of the pump beam. According to our findings on the photorefractive properties of SNP (Refs. 20 and 24) it is possible to generate refractive-index changes using light within the whole visible spectral range. However, recording in the red and near-infrared spectral range requires a pre-exposure to light, e.g., with a wavelength λ=488 nm and a polarization state $\vec{E}_p \| c$ in order to reach maximum population of the metastable state SI. Hence recording is performed by depopulation of the metastable states (erase mode).

Figure 4 shows the scattering patterns for the RGB wavelengths λ_p=457.9, 532, and 632.8 nm ($\vec{E}_p \| \vec{E}_r \| a$) in a *b* cut of thickness d=210 μm. The appearance of the scattering was also observed for λ_p=476, 488, 501, 780, and 1064 nm.

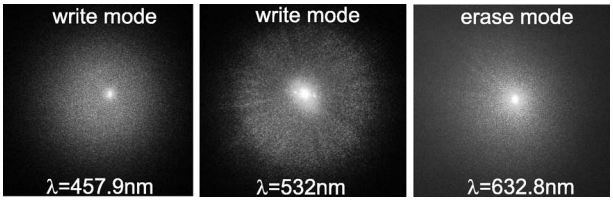

FIG. 4. Photographs of the scattering distributions taken on a screen behind the crystal in the write mode at λ_p=457.9 and 532 nm, Q=100 W s/cm^2, and in the erase mode at λ_p=632.8 nm, Q=5 W s/cm^2. Light polarization for read-out was chosen $\vec{E}_r \| a$.

In the second part of our investigation we focus on the spatial intensity distribution of the scattering pattern. In Fig. 5 the normalized intensity of the scattered light I_S as a function of the internal apex angle θ (*c* cut, d=210 μm, $\vec{E}_r \| a$, scan ∥ b axis) after exposure to laser light with a wavelength λ_p=532 nm and $\vec{E}_p \| a$ (Q=894 W s/cm^2) is depicted (black symbols). The initial intensity distribution recorded at the beginning of the exposure is shown for comparison (grey symbols). Both data sets are normalized to the transmitted intensity at θ=0°, where the diode passes the pump beam, so that the increase of the scattered light is corrected for absorption. The internal scattering angle θ is calculated considering Snell's law and a refractive index n_a=1.6320 (λ=532 nm). The intensity distribution recorded at the very beginning of exposure reflects the Gaussian profile of the directly transmitted laser beam and a distribution of scattered light with a very low intensity into a wide solid angle. This initially scattered light is usually attributed to incoherent scattering processes of the pump beam from inhomogeneities at the crystal surface and in the volume. The intensity distribution after exposure shows that the scattered light has increased tremendously and forms a broad maximum at an apex angle of $\theta^{\max} = \pm 8.0°$.

In order to check for the symmetry of the scattered light with respect to the ±*b* axis, i.e., ±θ, we evaluated the asymmetry parameter

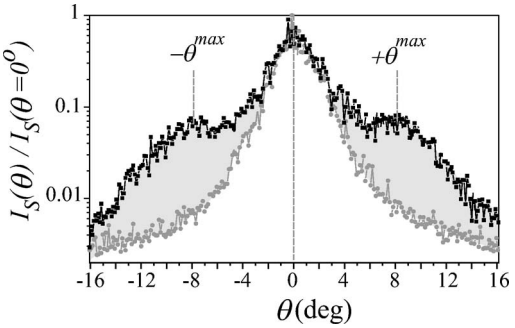

FIG. 5. Logarithmic plot of the intensity of the transmitted laser light as a function of the internal apex angle θ for Q=0 W s/cm^2 (grey symbols) and Q=894 W s/cm^2 (black symbols). The spectra are normalized to the maximum value at θ=0°, where the Si-PIN diode passes the directly transmitted laser beam. A maximum of the scattered light is observed at $\theta^{\max} = \pm 8.0°$. The grey hatched area corresponds to the integrated scattered intensity $\bar{I}_S$ [see Eq. (2)]. Experimental configuration: *c* cut of thickness d=210 μm, $\vec{E}_p$ and $\vec{E}_r \| a$ axis, λ_p=532 nm.

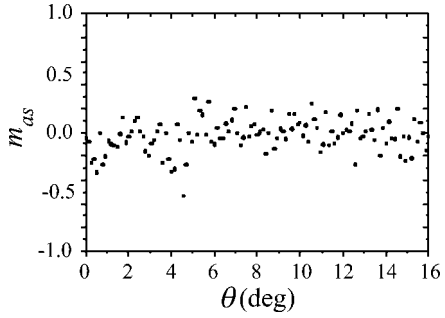

FIG. 6. Asymmetry parameter m_{as} as a function of the apex angle determined from the spatial intensity distribution in Fig. 5.

$$m_{\mathrm{as}}(\theta) = \frac{I_S(+\theta) - I_S(-\theta)}{I_S(+\theta) + I_S(-\theta)} \tag{1}$$

for the data presented in Fig. 5.

In the present case a symmetric distribution, tantamount to $m_{\mathrm{as}}(\theta)=0$, is found within the experimental error at all apex angles (Fig. 6). Additionally scans along the a axis with $\vec{E}_p \| a$, $\vec{E}_r \| a$ were performed. Analogous results were obtained. The same holds for intensity scans $\| a$ and b axis with light polarizations $\vec{E}_p \| b$, $\vec{E}_r \| b$. Therefore, we conclude that the observed scattering distributions are radially symmetric around the directly transmitted laser beam.

In order to estimate the efficiency of the scattering process we determined the integrated scattering efficiency

$$\bar{\eta}_S := \frac{\bar{I}_S}{\bar{I}_S + I_T}. \tag{2}$$

Here, I_T denotes the intensity of the transmitted laser beam and $\bar{I}_S$ is the integrated scattered intensity derived from the data in Fig. 5 by subtraction of the two spectra from each other and subsequent integration over the angle θ. Thus, $\bar{\eta}_S$ describes the degree of the pump beam intensity diffracted at the parasitically recorded phase gratings in the plane of scan direction and wave vector of the pump beam. If the pump beam becomes more and more depleted $\bar{\eta}_S$ approaches unity. For the experimental data of Fig. 5 we get $\bar{\eta}_S=(0.3\pm0.04)$, i.e., about 30% of the transmitted light is found in the scattering pattern.

The spatial distribution of the scattering intensity $I_S(\theta)$ was investigated repeatedly as a function of exposure up to $Q=3300$ W s/cm^2. Then the asymmetry parameter and the integrated scattering efficiency were evaluated for each spectrum. A dependence of the asymmetry parameter on exposure for the scattering patterns did not occur, whereas a remarkable development of $\bar{\eta}_S(Q)$ could be observed as shown in Fig. 7.

At the beginning the integrated scattering efficiency increases, passes a maximum value of $\bar{\eta}_S=(0.47\pm0.05)$ at $Q_{\mathrm{max}}=(420\pm40)$ W s/cm^2, and decreases to a saturation value of $\bar{\eta}_S=(0.1\pm0.01)$ upon further exposure. The data indicate that the scattering vanishes completely for $Q\to\infty$.

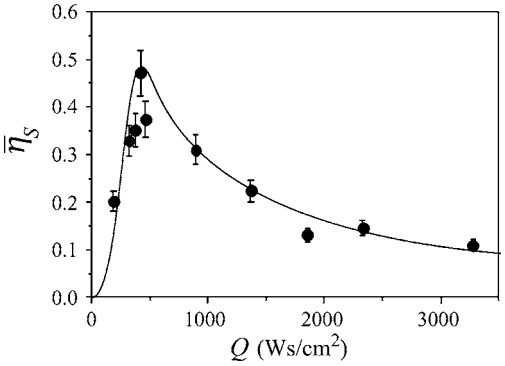

FIG. 7. Integrated scattering efficiency $\bar{\eta}_S$ as a function of exposure determined from the spatial intensity distributions. Same configuration as for Fig. 5. The solid line is a guide to the eyes.

However, this could not be verified experimentally due to the limited durability of the nitrogen filled Dewar.

We found that the characteristic measure Q_{max}, i.e., the exposure at the maximum scattering intensity, is a function of beam diameter, wavelength, apex angle and of crystal thickness. Figure 8 exemplarily illustrates the kinetics of the scattering intensity observed in a SNP crystal of thickness $d=340$ μm exposed to a particular pump beam intensity of $I=270$ mW/cm^2 and pump beam diameter of 2.1 mm for two different wavelengths $\lambda=532$ and 514 nm.

The measurement was performed using a Si-PIN diode at a fixed angular position of $\theta=8°$ and yielded $Q_{\mathrm{max}}(532\ \mathrm{nm})=(100\pm4)$ W s/cm^2 and $Q_{\mathrm{max}}(514\ \mathrm{nm})=(66\pm3)$W s/cm^2, respectively. Note, that the angular position of the maximum scattered intensity of $\theta^{\mathrm{max}}=8°$ (see Fig. 5) did not alter for the two wavelengths. Hence, Q_{max} differs by a factor of ≈1.5 due to the shift of 18 nm in the pump beam wavelength. This is attributed unambiguously to the population kinetics of the metastable states, as a ratio of ≈1.5 was reported between $\lambda_p=532$ nm and $\lambda_p=514$ nm for Q_{max}.[29]

Figure 9 shows the dependence of Q_{max} on the apex angle for $\lambda_p=532$ nm, i.e., the kinetics of the scatter-

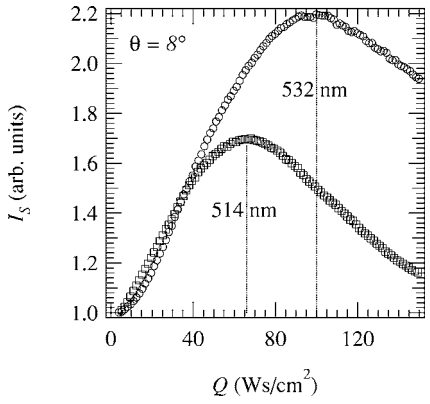

FIG. 8. Intensity of scattered light measured at an apex angle of $\theta=8°$ as a function of exposure in a SNP b cut of thickness $d=340$ μm for $\lambda=514$ nm and $\lambda=532$ nm. The intensities are normalized to the initial scattering intensity at $Q=0$ W s/cm^2. Beam diameter of the pump beam of 2.1 mm and pump beam intensity of $I=270$ mW/cm^2.

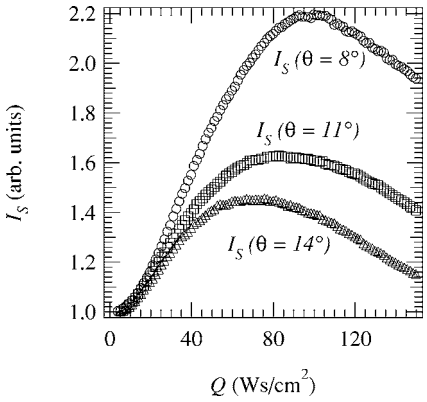

FIG. 9. Intensity of the scattered light I_S for three apex angles $\theta=8°$, 11°, 14° as a function of exposure. The intensities are normalized to the initial scattering intensity at $Q=0$ W s/cm^2. $I_p=270$ mW/cm^2, $\vec{E}_p \| a$ axis, $\lambda_p=532$ nm, b cut, $d=340$ μm.

ing intensity was investigated for three apex angles $\theta=8°$, $\theta=11°$, and $\theta=14°$. Obviously, the exposure at which the maximum of the scattered intensity is reached in this range differs: $Q_{\max}(8°)=(100\pm4)$ W s/cm^2, $Q_{\max}(11°)=(82\pm5)$ W s/cm^2, and $Q_{\max}(14°)=(71\pm4)$ W s/cm^2. Measurements of the intensities at corresponding symmetric angles $\theta=-8°, -11°, -14°$ showed an analogous behavior.

The kinetics determined from the investigation of the integral scattered intensity (Fig. 7) and of the scattered intensity at the angular position of the maximum intensity (Fig. 8), respectively, show a clear difference with respect to $Q_{\max}$. This is primarily a result of both the different pump beam diameter and the crystal thickness: At the same wavelength of 532 nm, but with different beam diameters and crystal thicknesses of 5.9 mm and $d=210$ μm (Fig. 7) and of 2.1 mm and $d=340$ μm (Fig. 8), a ratio of approximately five between the respective values of $Q_{\max}$ occurs.

IV. DISCUSSION

The build-up of scattered light upon exposure to a coherent laser beam in centrosymmetric crystals of SNP has already been attributed to the recording of parasitic holographic phase gratings via the detection of scattering cones.[7] Such volume phase holograms can be recorded in SNP single crystals via the particular photorefractive effect originating from the generation of metastable states located at $[Fe(CN)_5NO]^{2-}$-molecules (NP molecules) as light-induced linkage isomers of the NO ligand.[30] A comprehensive study of this photorefractive effect, that is not at all related to electrooptics, is presented in Ref. 20.

The close relation between the photorefractive response in SNP and the light-induced generation of metastable electronic states enforces a causal connection between holographic light scattering and the metastable states. This interrelation is reflected in the dependence of the scattered light on the light polarization of pump and readout beam, on the wavelength and exposure dependencies, as demonstrated by the presented experimental results.

Three remarkable peculiarities of the scattering are found, which cannot be explained within this context. (A) Readout of the scattering pattern is forbidden choosing a light polarization $\vec{E}_r \| c$ axis. (B) The kinetics of the scattered light intensity shows a transient behavior. (C) The scattering corona is identified as a broad ring surrounding the directly transmitted laser beam. In the following we will discuss item (A) in the frame of the geometrical alignment of the NP molecules within the crystal unit cell and issues (B) and (C) in the frame of the nonlinear photorefractive response.

A. Scattering pattern and light polarization states

The results of Fig. 3 show that readout of the scattering process is impossible whenever choosing a light polarization $\vec{E}_r \| c$ axis. This result is unexpected as the maximum population of the metastable state SI of $P_{SI} \approx 50\%$ can be achieved in this configuration:[29] Following the attempt given in Ref. 20, i.e., that there is a linear dependence of the photoinduced refractive-index modulation on the population, the largest photorefractive response is expected for the $\vec{E}_r \| c$ axis. At the same time the most pronounced scattering process should occur choosing a light polarization $\vec{E}_p$ and $\vec{E}_r \| c$ axis of pump and readout beam.

The complete absence of scattering for $\vec{E}_p$ and $\vec{E}_r \| c$ and the unique possibility to control its appearance via the light polarization of the readout beam (see Fig. 3) can be explained by the existence of latent holographic phase gratings. In the context of SNP these are phase gratings recorded with $\vec{E}_p \| c$ that cannot be reconstructed using light of the same polarization state ($\vec{E}_r \| c$). On the other hand, diffraction occurs with light polarized $\vec{E}_r \| a$ or b axis. The presence of latent gratings with such properties has been demonstrated unambiguously in SNP for recording an elementary holographic phase grating.[20] As the scattering is shown to result from diffraction at a multitude of volume phase gratings, the discovered characteristic polarization dependence of the scattering pattern reflects and even proves the presence of parasitically recorded latent holographic phase gratings.

The existence of latent volume phase gratings results from the geometrical alignment of the $[Fe(CN)_2NO]^{2-}$ anions in the orthorhombic unit cell of SNP. Here, their quasifourfold N-C-Fe-N-O symmetry axis lies in the a-b-mirror plane. The generation of the metastable states is connected with a structural rearrangement of the Fe-N-O group, which is confined to the a-b-mirror plane for the metastable state SI.[30–32] Hence the changes of the electronic polarizability of the molecules along the N-C-Fe-N-O axis, which induce a refractive-index change via the Lorentz-Lorenz relation, are modified exclusively within the a-b-mirror plane. As a result the corresponding refractive-index changes $\Delta n_a \neq 0$, $\Delta n_b \neq 0$, and $\Delta n_c = 0$ upon optical excitation of SI with $\vec{E}_p \| c$. This interpretation is supported by holographic experiments on $Ba[Fe(CN)_5NO] \cdot 3H_2O$, where the $[Fe(CN)_5NO]^{2-}$ anions do not have this characteristic orientation of the quasifourfold N-C-Fe-N-O axis, and hence latent gratings could not be found. In contrary gratings could be recorded and read out with any polarization state of light.[33]

B. Kinetics of scattering

A second feature of the scattering process that does not reflect the properties of excited metastable states is the kinet-

ics of the scattering intensities during exposure. The population of the metastable states follows a monoexponential law upon exposure as a result of an optically induced transfer between ground state and metastable state of the NP molecule (see Ref. 29). The kinetics of the scattered intensity, however, shows a characteristic transient behavior: It increases, passes a maximum and finally saturates, even vanishes for large exposure.

Such a transient behavior of grating recording is commonly explained by assuming the presence of compensating gratings[34] or a transient energy exchange.[35] Recording of compensating gratings is based on the assumption that two independent gratings with different characteristic time constants evolve, but are phase shifted by π and hence compensate each other. The diffraction efficiency of compensating gratings and its kinetics depend on the maximum amplitude of the refractive-index modulation (or of the absorption coefficient) as well as on the individual recording kinetics of the two gratings. Therefore a transient behavior and a nonzero saturation value of the diffraction efficiency can result.

To find an explanation for the transient kinetics of hologram recording in the two-beam setup, the existence of compensating gratings was discussed in SNP. This seemed reasonable as two metastable states (SI, SII) can be generated simultaneously.[20] However, contrary to $Ba[Fe(CN)_5NO]\cdot 3H_2O$ this explanation was discarded after performing particular experiments: after recording to the steady state, i.e., zero diffraction efficiency, the diffraction efficiency did not increase again upon selective erasure of one of the possible grating components (SII). In addition, a photoinduced refractive-index change was not observed in the visible spectral range upon generation of only state SII. Even contrary, grating recording by exciting state SI is accompanied by refractive-index changes up to a maximum value of $n_1 \approx 1.4\times 10^{-2}$ at a pump beam wavelength of $\lambda = 514$ nm.[20,36]

Therefore, we anticipate that compensating gratings can likewise be ruled out to explain the kinetics of the scattering intensity. This assumption is also supported by the temperature dependent investigations of the scattering: The decay of the scattering intensity shows a maximum at $T \approx 195$ K, whereas there are no changes of the scattering passing $T \approx 140$ K. By comparing these findings to the corresponding decay temperatures of the mestastable states SI ($T=190$ K) and SII ($T=140$ K),[37] it is obvious, that the scattering is significantly connected with SI. A contribution of SII thus can be ruled out—in accordance with the results of elementary grating recording.

The observed kinetics of the scattering process resemble that in the case of a transient energy exchange as well.[35] A transient energy exchange takes place during grating recording with a modulation depth of the incoming light interference pattern of $m=2\sqrt{I_R I_S}/(I_R+I_S)\neq 1$ and a local, noninstantaneous photorefractive response. In this case the recorded gratings and the interference pattern become dephased with increasing refractive-index modulation as a function of the propagation coordinate, and we finally end up with a slanted grating and equal intensities. During the build-up beam coupling is allowed, i.e., a transient energy exchange from the strong to the weak beam occurs, that vanishes in the steady state.

The scattering in SNP fulfills all requirements for a transient energy exchange as a low modulation depth $m \ll 1$ of the incoming light interference pattern is to be expected due to the large intensity ratio between pump beam and initially scattered waves. In addition the photorefractive response in SNP is local.[20] However, in the two-beam setup the appearance of a transient energy exchange was ruled out to explain the transient kinetics of hologram recording. It was shown that the transient behavior of the diffraction efficiency appears even when the modulation depth is $m=1$.[20] We performed rocking curves during recording with $m\neq 1$ to detect a tentative slant angle of elementary gratings, but could not find any indication for the presence of such a slant. This additionally suggests that transient energy transfer might be neglected in this case. The reason for the absence of transient energy transfer remains an interesting unsolved topic for further investigations, and possibly could be a result of the very thin crystal samples ($d \ll 500$ μm).

Only recently, we introduced a new model to explain transient kinetics of hologram recording in media with a local photorefractive response.[38] There we consider a nonlinear photorefractive response (NLPR) and—contrary to compensating gratings or transient energy transfer—are able to successfully describe the entire set of experimental results for the hologram recording kinetics in SNP very well, including that of the modulation depth dependence and in particular the case $m=1$.

The NLPR model is applicable to materials assembled from photoswitchable compounds with two long-lived (meta)stable states. Considering a photoinduced transfer between the two states (GS,SI), the kinetics of their population p is governed by a system of linear differential equations

$$\frac{dp_i}{dt} = (-\gamma_i p_i + \gamma_j p_j) I, \quad i \neq j = \{GS, SI\}. \tag{3}$$

Here, γ denote reaction constants and I the intensity of the light. The solution yields a monoexponential dependence on exposure for the population of each state. In this case, the sinusoidal interference pattern $I(x)=I_0[1+m\cos(Kx)]$ generates an initially sinusoidal spatial modulation of the population which is strongly deformed upon further exposure and finally we end up with a spatially homogeneous population in the steady state. Assuming a linear dependence between the population and the amplitude of the refractive-index change results in the same kinetics for the spatial modulation $n(t,x) \propto (p_{GS}-p_{SI}) = n(t=0)+\Delta n \exp\{-\gamma I(x) t\}$: starting with a sinusoidal modulation of the refractive index, the latter becomes homogeneous for long exposure $Q=I_0 t$, however, is different from the initial refractive index. Expansion in a Fourier series leads to

$$n(q,x) = n(t=0) + \Delta n \times \left(\mathcal{I}_0(mq) + 2\sum_{s=1}^{\infty} (-1)^s \mathcal{I}_s(mq) \cos(sKx) \right) e^{-q}, \tag{4}$$

with the normalized exposure $q=Q\gamma$, Δn the total refractive-

index change, and $\mathcal{I}_s$ the sth order modified Bessel function of the first kind. Therefore, the kinetics of the first (and higher) order diffraction efficiency is as follows: for low exposure it increases, then passes a maximum, decreases and finally approaches zero for long exposure, i.e., a transient kinetics of hologram recording appears.

An important consequence that arises from this model is the prediction that inevitably higher harmonics in the Fourier expansion of the refractive-index appear. Performing diffraction experiments, the scattering amplitude thus will be nonzero at multiples of the fundamental grating vector $\vec{K}$. Hence readout of the gratings with vector $2\vec{K},3\vec{K},\ldots$, should be possible and is a key proof for the presence of this recording mechanism.

To consider the NLPR-model for the kinetics of hologram recording in SNP, the material has to comply with the model requirements: Obviously, the optically switchable compounds are represented by the NP molecule having the possibility of a photoinduced transfer between ground state and metastable state SI. The NP molecule can be regarded as stable in both of these states at temperatures below $T=135$ K as the lifetime of SI is more than 10^9 s.[39] The monoexponential behavior of the population is experimentally proven[29] and a linear dependence between population and the amplitude of the refractive-index modulation can be well assumed. The constant multiplicative factor was already experimentally estimated to $c=0.12$ (see Ref. [20]).

In Ref. 38 it was shown, that the function describing the grating kinetics derived from the NLPR model can be well fitted to the experimental data set of hologram recording in SNP, even for low modulation depths. Further, the appearance of $2\vec{K}$ gratings was observed by detecting the respective diffraction efficiency,[40] thus additionally proving the applicability of the model to SNP.

In the following we hence assume that the scattering kinetics in SNP is exclusively determined by the nonlinear photorefractive response, i.e., we neglect the contribution of transient energy exchanges in the following. This allows us to discuss any process in SNP based on the NLPR model, that contributes to the appearance of scattering and their respective properties.

In the frame of the common conception for the build-up of photoinduced light scattering it is interesting to discuss the influence of waves diffracted at $2\vec{K},3\vec{K},\ldots$, gratings. For convenience, we will restrict ourselves to $2\vec{K}$ gratings, but the considerations below apply also to diffraction at $3\vec{K},4\vec{K},\ldots$, gratings. We start with discussing a sketch of the wave vector and grating vector configuration in the reciprocal space (Fig. 10). The pump beam with wave vector $\vec{k}_p$ and an initially scattered wave $\vec{k}_s^{(a)}$ record a grating with Bragg angle $\theta^{(1)}$ and grating vector $\vec{K}^{(1)}$. Because of the nonlinear response at the same time a grating with vector $\vec{K}^{(2)}=2\vec{K}^{(1)}$ is generated. Diffraction of a scattered wave $k_s^{(b)}$ from the latter only occurs, if the condition $\vec{k}_s^{(b)}-\vec{K}^{(2)}=\vec{k}_d$ is fulfilled. As a remarkable result the diffracted wave $\vec{k}_d$ records another grating with a grating vector $\vec{K}^{\Delta}=\vec{k}_p-\vec{k}_d$ by interference with the pump beam. We emphasize, that this process will lead by and

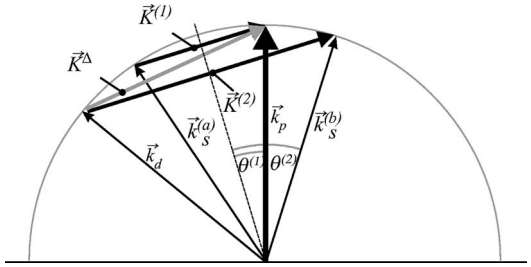

FIG. 10. Ewald construction for recording parasitic holographic gratings by diffraction processes of scattered waves from grating vectors with multiple spatial frequency.

by to wide angle scattering even without the existence of initially scattered light along those directions. In other words: waves diffracted at $2\vec{K}$ gratings act as initially scattered waves without the presence of further scattering centers, in contrast to the assumptions of the common concept.[18] Hence, wide-angle photoinduced scattering might appear even in materials with excellent optical quality. We assume, that initial recording of parasitic gratings at very small angles is a result of the pump-beam divergence.

The efficiency of such a process strongly depends on the diffraction efficiency of the $2\vec{K}$-grating component. With the results presented in Ref. 38 we can get insight to the ratio of the diffraction efficiencies of the $\vec{K}$- and $2\vec{K}$-grating component for SNP. The particular case of an elementary phase grating recorded with a modulation depth of $m=0.089$, yields $\eta(\vec{K}):\eta(2\vec{K})=500:1$ at the exposure where the $2\vec{K}$-grating component passes its maximum. Or, for a maximum value of $\eta(\vec{K})=2.0\%$ we get a maximum value of $\eta(2\vec{K})\approx 0.002\%$, i.e., 2 μW is diffracted from the $2\vec{K}$-grating component with an incoming laser power of 100 mW.

The appearance of initially scattered light from $2\vec{K}$ gratings will affect the kinetics of the build-up of light scattering as well. The scattering will first start with scattered light under small angles around the forward direction, followed by fanning to large apex angles due to the processes described above. Obviously, this fanning initiated by the appearance of $2\vec{K}$ gratings is predominant in the absence of initially scattered light originating from imperfections of the crystal surface or the bulk and for large apex angles as well. However, the underlying data set of Fig. 9 shows sufficient intensity at all three apex angles at the beginning of the exposure with an intensity ratio of $I_{S0}(8°):I_{S0}(11°):I_{S0}(14°)=2.4:1.4:1$. This agrees with the initial intensity distribution illustrated in Fig. 5. Hence the direct recording of $\vec{K}$ gratings by optical noise inherent in the crystal dominates the scattering kinetics at the investigated angles, so that we did not observe the predicted fanning effect in SNP. Here, investigations of the scattering kinetics at angles $\gg 14°$ or in materials with a nonlinear photorefractive response and high optical quality seem to be more promising.

The decrease of initially scattered light intensity with increasing apex angle $I_{S0}(\theta)$ gives rise to an angular distribution of the modulation depth $m(\theta)=2\sqrt{I_p I_{S0}(\theta)}/[I_p+I_{S0}(\theta)]$.

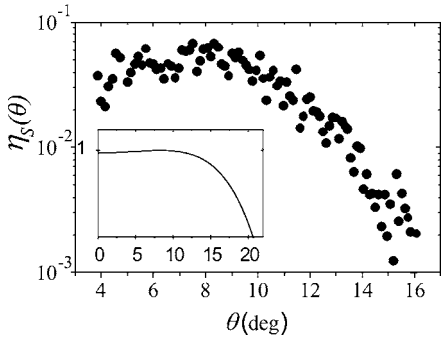

FIG. 11. Scattering efficiency as a function of the internal scattering angle θ evaluated from the experimental data in Fig. 5. Inset: Dependence of the diffraction efficiency on the slant angle for a lossless dielectric grating (Ref. 42).

The NLPR model predicts, that m significantly affects the maximum value of the diffraction efficiency, but only slightly the value of $Q_{\max}$[38]. The data of Fig. 9 are fully consistent with these predictions: the maximum amplitude of the scattering significantly differs by a factor of ≈ 1.6, whereas $Q_{\max}$ changes by less than ±20% for the three investigated apex angles.

C. Spatial scattering intensity distribution

We can now discuss the third particularity of our experimental findings: the occurrence of an intense broad scattering ring surrounding the directly transmitted laser beam. Characteristic spatial distributions of the intensity of the scattered light are well known from photoinduced light scattering originating from the angular dependence of the small signal amplification gain.[41] As we exclude beam-coupling processes, the angular dependence of the scattered light intensity I_S in SNP (see Fig. 5) essentially stems from diffraction processes of the pump beam at a multitude of parasitically recorded gratings. We can neglect the contribution of waves diffracted at $2\vec{K},3\vec{K},\ldots$, gratings to I_S according to the intensity ratio of the respective diffracted waves. For the same reason we exclude interaction processes between waves diffracted at $\vec{K},2\vec{K},3\vec{K},\ldots$, gratings.

Hence, $I_S(\theta)$ predominately is a result of the angular dependence of the diffraction efficiency $\eta(\theta)$ of the $\vec{K}$ gratings. It should be noted that this attempt is confirmed by our previous considerations to the angular dependence of the scattering kinetics. Using the experimental data shown in Fig. 5, we determine the scattering efficiency for the particular exposure of $Q=894$ Ws/cm^2 defined as

$$\eta_S(\theta) = \frac{I_S(\theta) - I_{S0}(\theta)}{I_P}. \tag{5}$$

Here, $I_S(\theta)$ is the intensity of the scattering corona, $I_{S0}(\theta)$ is the intensity at zero exposure, and I_P is the intensity of the pump beam. The dependence $\eta_S(\theta)$ is shown in Fig. 11 in the angular range 3.8°–16.2°, where the influence of the pump beam is negligible.

For comparison the inset shows the qualitative dependence of the diffraction efficiency for the case of slanted elementary phase gratings given from Ref. 42 via the relation

$$\eta(\theta) = \frac{I_d(\theta)}{I_P} \sim \sin^2\left(\frac{\pi n_1 d}{\lambda\sqrt{1-2\sin^2(\theta/2)}}\right). \tag{6}$$

Here, n_1 denotes the amplitude of the first Fourier component of the refractive index, d the hologram thickness, and θ is connected to the Bragg angle via $\theta=2\Theta_B$. I_d and I_P are the intensities of the diffracted and incoming waves, respectively. Inspecting Eq. (6) a maximum can be found at $\theta_{\max}(n_1)=\arcsin[\sqrt{(\lambda^2-4n_1^2d^2)/2\lambda^2}]$.

The qualitative agreement between the determined angular dependence of the scattering and diffraction efficiency is obvious. Further attempts to describe $\eta(\theta)$ more precisely will have to consider the angular dependence of n_1 as well. We expect such a dependence $n_1(\theta)$ by combining the following two experimentally found aspects: (a) a dependence of the photoinduced refractive-index amplitude on the modulation depth $n_1(m)$ was found experimentally in the two-beam setup[20] and (b) the angular distribution of the initial scattered light (see Fig. 5) gives strong evidence for an angular dependence of the modulation depth $m(\theta)$.

We summarize, that the proposed concept for the build-up of initial scattering due to the presence of $2\vec{K},3\vec{K},\ldots$, gratings as well as the assumptions made comply with the experimental findings and the respective analysis. The kinetics of the scattering can be explained by the NLPR model and the scattering corona can be regarded to originate from diffraction processes of the pump beam at parasitically recorded $\vec{K}$ gratings. We emphasize again, that there is no need for taking beam-coupling processes into account to describe our experimental findings. This—and the fact that the linear electrooptic effect is not responsible for the photorefractive response—strongly discriminates the scattering phenomenon observed in SNP from the well-known phenomenon of photoinduced light scattering observed in electrooptic crystals.[8] The more general designation holographic light scattering is proper for this specific kind of light scattering in order to separate the different phenomena.

V. CONCLUSION

In conclusion we have found three more interesting features of light-induced scattering in centrosymmetric SNP. The possibility to switch scattering patterns on and off by simply changing the polarization state of the read-out beam unambiguously results from the interrelation between photorefraction and structural changes of the Fe-N-O binding, which are restricted to the a-b-mirror plane. The kinetics and spatial distribution of the scattering pattern can be explained on the basis of two-beam interaction processes. An approach for three-wave interaction including diffraction processes from higher harmonics is discussed to explain the build-up of wide-angle scattering.

ACKNOWLEDGMENTS

Financial support by the Deutsche Forschungsgemeinschaft (DFG, Project No. IM 37/2-1, GRK 695, and WO 618/5-3) and of the Fonds zur Förderung der wissenschaftlichen Forschung (FWF, Project No. P15642) is acknowledged. Martin Fally is grateful for a visiting professorship within the Mercator programme funded by the DFG (Grant No. OS 55/12-1).

*Permanent address: Nonlinear Physics group, Faculty of Physics, Vienna University, Austria

†Electronic mail: mimlau@uos.de http://www.mimlau.de

[1] A. Ashkin, G. D. Boyd, J. M. Dziedzic, R. G. Smith, A. A. Ballman, A. A. Levinstein, and K. Nassau, Appl. Phys. Lett. **9**, 72 (1966).

[2] R. Magnusson and T. K. Gaylord, Appl. Opt. **13**, 1545 (1974).

[3] M. R. B. Forshaw, Opt. Commun. **8**, 201 (1973).

[4] J. M. Moran and I. P. Kaminow, Appl. Opt. **12**, 1964 (1973).

[5] M. A. Ellabban, M. Fally, H. Uršič, and I. Drevenšek-Olenik, Appl. Phys. Lett. **87**, 151101 (2005).

[6] A. V. Knyazkov, M. N. Lobanov, A. Krumins, and J. Seglins, Ferroelectrics **69**, 81 (1986).

[7] M. Imlau, T. Woike, R. Schieder, and R. A. Rupp, Phys. Rev. Lett. **82**, 2860 (1999).

[8] V. V. Voronov, I. R. Dorosh, Y. S. Kuz'minov, and N. V. Tkachenko, Sov. J. Quantum Electron. **10**, 1346 (1980).

[9] M. Imlau, M. Goulkov, M. Fally, and T. Woike, in *Polar Oxides: Properties, Characterization and Imaging*, edited by R. Waser, U. Böttger, and S. Tiedke (Wiley-VCH, Weinheim, 2005), Chap. 9, pp. 163–188.

[10] H. Zöllner, W. Krasser, Th. Woike, and S. Haussühl, Chem. Phys. Lett. **161**, 497 (1989).

[11] K. Ookubo, Y. Morioka, H. Tomizawa, and E. Miki, J. Mol. Struct. **379**, 241 (1996).

[12] P. Gütlich, Y. Garcia, and Th. Woike, Coord. Chem. Rev. **219-221**, 839 (2001).

[13] P. Coppens, I. Novozhilova, and A. Kovalevsky, Chem. Rev. (Washington, D.C.) **102**, 861 (2002).

[14] E. Culoota and D. E. Koshland, Science **258**, 1862 (1992).

[15] J. S. Stamler, D. J. Singel, and J. Loscalzo, Science **258**, 1898 (1992).

[16] L. Ignarro and F. Murad, *Nitric Oxide: Biochemistry, Molecular Biology, and Therapeutic Implications, Advances in Pharmacology* (Academic, New York, 1995), Vol. 34.

[17] D. Schaniel, M. Imlau, Th. Weisemoeller, Th. Woike, K. W. Krämer, and H. U. Güdel, (unpublished).

[18] R. A. Rupp and F. W. Drees, Am. J. Otolaryngol. **39**, 223 (1986).

[19] N. V. Kukhtarev, V. B. Markov, S. G. Odulov, M. S. Soskin, and V. L. Vinetskii, Ferroelectrics **22**, 961 (1979).

[20] M. Imlau, S. Haussühl, T. Woike, R. Schieder, V. Angelov, R. A. Rupp, and K. Schwarz, Appl. Phys. B: Lasers Opt. **68**, 877 (1999).

[21] M. Goulkov, S. Odoulov, T. Woike, J. Imbrock, M. Imlau, E. Krätzig, C. Bäumer, and H. Hesse, Phys. Rev. B **65**, 195111 (2002).

[22] M. Y. Goulkov, T. Granzow, U. Dörfler, T. Woike, M. Imlau, and R. Pankrath, Appl. Phys. B: Lasers Opt. **76**, 407 (2003).

[23] M. Goulkov, M. Imlau, R. Pankrath, T. Granzow, U. Dörfler, and T. Woike, J. Opt. Soc. Am. B **20**, 307 (2003b).

[24] T. Woike, S. Haussühl, B. Sugg, R. A. Rupp, J. Beckers, M. Imlau, and R. Schieder, Appl. Phys. B: Lasers Opt. **63**, 243 (1996).

[25] U. Hauser, V. Oestreich, and H. D. Rohrweck, Z. Phys. A **280**, 17 (1977).

[26] A. M. Glass, Opt. Eng. **17**, 470 (1978).

[27] M. Imlau, R. Schieder, R. A. Rupp, and T. Woike, Appl. Phys. Lett. **75**, 16 (1999).

[28] T. Manoharan and W. C. Hamilton, Inorg. Chem. **2**, 1043 (1963).

[29] T. Woike, W. Krasser, H. Zöllner, W. Kirchner, and S. Haussühl, Z. Phys. D: At., Mol. Clusters **25**, 351 (1993).

[30] M. Carducci, M. Pressprich, and P. Coppens, J. Am. Chem. Soc. **119**, 2669 (1997).

[31] M. Rüdlinger, J. Schefer, C. Chevrier, N. Furer, H. U. Güdel, S. Haussühl, G. Heger, P. Schweiss, T. Vogt, T. Woike, and H. Zöllner, Z. Phys. B: Condens. Matter **83**, 125 (1991).

[32] D. Schaniel, J. Schefer, M. Imlau, and T. Woike, Phys. Rev. B **68**, 104108 (2003).

[33] T. Woike, M. Imlau, S. Haussühl, R. A. Rupp, and R. Schieder, Phys. Rev. B **58**, 8411 (1998).

[34] X. Yue, J. Xu, F. Mersch, R. A. Rupp, and E. Krätzig, Phys. Rev. B **55**, 9495 (1997).

[35] V. L. Vinetskiĭ, N. V. Kukhtarev, S. G. Odulov, and M. S. Soskin, Sov. Phys. Usp. **22**, 742 (1979).

[36] M. Imlau, T. Woike, D. Schaniel, J. Schefer, M. Fally, and R. A. Rupp, Opt. Lett. **27**, 2185 (2002).

[37] D. Schaniel, T. Woike, L. Tsankov, and M. Imlau, Thermochim. Acta **429**, 19 (2005).

[38] M. Fally, M. Imlau, R. A. Rupp, M. A. Ellabban, and T. Woike, Phys. Rev. Lett. **93**, 243903 (2004).

[39] H. Zöllner, T. Woike, W. Krasser, and S. Haussühl, Z. Kristallogr. **188**, 139 (1989).

[40] M. Imlau, S. Hausfeld, and M. Fally (unpublished).

[41] M. Goulkov, T. Granzow, U. Dörfler, T. Woike, M. Imlau, R. Pankrath, and W. Kleemann, Opt. Commun. **218**, 173 (2003).

[42] H. Kogelnik, Bell Syst. Tech. J. **48**, 2909 (1969).